

Coherent Anti-Stokes Emission in a Continuous Wave Raman Laser in H₂

J.K. Brasseur *, P.A. Roos, K.S. Repasky and J.L. Carlsten
Department of Physics
Montana State University
Bozeman MT., 59717

e-mail: Jay.Brasseur@usafa.af.mil, roos@physics.montana.edu,
repasky@physics.montana.edu, and carlsten@physics.montana.edu

* J.K. Brasseur is now with the Department of Physics, Laser and Optics Research
Center, USAFA, CO 80840

We report the observation of cw coherent anti-Stokes emission from a non-resonant cw Raman laser in H₂. The anti-Stokes emission is co-linear with the pump and Stokes beams with a gaussian spatial profile. The external anti-Stokes to Stokes power ratio is 26.3ppm when the laser cavity is tuned to the center of the Raman resonance and higher for slight detuning from line center. A steady-state theory is presented which accurately describes the anti-Stokes behavior as a function of output Stokes power and detuning from the Raman resonance.

1. Introduction

Using the high optical power build-up within a high finesse cavity (HFC), it is now possible to study multi-photon nonlinear processes using low power continuous wave (cw) lasers for the driving fields. In particular, stimulated Raman scattering has recently been used to create non-resonant cw Raman lasers with pump thresholds on the order of 1mW [1-6]. In the previous work, HFCs allowed incident pump photons to generate red-shifted Stokes photons via molecular vibration in H₂.

Although these studies were limited to Stokes emission, additional parametric processes are also possible. Specifically, the four-photon coherent Raman anti-Stokes process has traditionally accompanied observation of Stokes emission in the high power regime[7-11]. Figure-1 illustrates the four-wave mixing process in which coherent anti-Stokes is produced. In the high-power pulsed regime, the observed anti-Stokes emission commonly exhibits a ring spatial pattern due to phase matching requirements between the pump, and the produced Stokes and anti-Stokes photons [12]. However, in cw Raman lasers, the strict HFC spatial mode selection allows only one spatial mode of the pump and the Stokes fields to resonate. To maximize the overlap of the pump and Stokes beams for gain purposes, fundamental Gaussian spatial modes are chosen, thereby prohibiting high-angle coherent anti-Stokes emission [1-6]. In this paper we characterize the properties of this emission with respect to the emitted Stokes power and the detuning from the Raman resonance.

This paper is organized in the following manner. Section 2 extends the cw Raman laser equations of reference 4 to include coherent anti-Stokes emission and examines the resulting steady-state limits. The effects of tuning the pump laser frequency

are also treated numerically in this section. Section 3 provides experimental verification of the presented steady-state theory, and section 4 contains some concluding remarks.

2. Theory

Using equations 1-4 of Ref. 13 (see also Ref. 12) and assuming a well-established polarization ($dQ/dt=0$), we extend the time-dependent cw Raman equations of Refs. 4 and 14 to include the four-wave mixing process for coherent anti-Stokes emission. This yields the following time dependent equations describing the fields inside the HFC:

$$\dot{E}_p = -L_p E_p - \frac{\omega_p}{\omega_s} G_s |E_s|^2 E_p + K(E_{p_{in}}, t) + G_p |E_{as}|^2 E_p \quad (1)$$

$$\dot{E}_s = -L_s E_s + G_s |E_p|^2 E_s + \frac{\omega_s}{\omega_{as}} C_{as}^{4W} E_p E_p E_{as}^* \quad (2)$$

$$\dot{E}_{as} = -L_{as} E_{as} - \frac{\omega_{as}}{\omega_p} G_p |E_p|^2 E_{as} - C_{as}^{4W} E_s^* E_p E_p \quad (3)$$

E_p , E_s , and E_{as} are the pump, Stokes, and anti-Stokes fields, and ω_p , ω_s , and ω_{as} are the pump, Stokes and anti-Stokes angular frequencies. Equation 3 describes the growth of the anti-Stokes field inside the HFC. The last term of equation 3 is due to the four-wave mixing process, where the negative sign denotes an 180° phase difference between the anti-Stokes field and the four-wave driving term. Coupling of the pump and Stokes fields to the anti-Stokes field, including phase-matching, for the four-wave mixing process is represented by C_{as}^{4W} . The second term of equation 3 attenuates the anti-Stokes field as seen in reference 12. This is a result of the normal Raman process where the anti-Stokes photon scatters inelastically to produce a photon at the pump frequency. Equations 1 and 2 are identical to the cw Raman laser equations of reference 4 with the four-wave mixing anti-Stokes process included.

The losses due to the mirrors are given by L_p , L_s , and L_{as} for the pump, Stokes and anti-Stokes frequencies respectively with the following functional form:

$$L = -\frac{c}{2\ell} \ln R \quad (4)$$

where ℓ is the cavity length, c is the speed of light, and R is the power reflectivity of the cavity mirrors at a given frequency. The rate at which the pump field enters the cavity is given by $K(E_{p_{in}}, t)$, as a function of the incident pump field $E_{p_{in}}$. The gains for the two-photon Raman processes are denoted by G_s and G_p for the Stokes and pump beams respectively. These gains are slightly different due to the different pumping field frequencies. We use the Lorentzian nature of the Raman linewidth to give the following detuning dependence of the Raman gain:

$$G(\Delta, \Gamma) = G \cdot \left(\frac{\left(\frac{\Gamma}{2}\right)^2}{\Delta^2 + \left(\frac{\Gamma}{2}\right)^2} \right) \quad (5)$$

where Δ is the detuning from the Raman resonance and Γ is the FWHM of the Raman resonance. Note when Δ is set to zero (line center) we recover the standard Raman gain, G .

For the steady-state limit, the time derivatives of the electric fields in equations 1-3 are set to zero. We can then solve for the steady-state values of the pump, Stokes and anti-Stokes fields. However, since the measured Stokes to anti-Stokes power ratio was on the order of 10-100 ppm, we use the steady-state results of reference 4 for the pump and Stokes steady-state fields. This essentially assumes the anti-Stokes field generation

does not significantly affect the pump and Stokes fields. Thus, using equation 3 we arrive at the following expression for the anti-Stokes field:

$$E_{as} = \frac{-C_{as}^{4W} E_p E_p E_s^*}{L_{as} + \frac{\omega_{as}}{\omega_p} G_p |E_p|^2}. \quad (6)$$

Assuming the reflectivity of the HFC mirrors at the anti-Stokes frequency is small

($R < 90\%$) ($L_{as} \gg \frac{\omega_{as}}{\omega_p} G_p |E_p|^2$), equation 6 can be reduced to the following expression

for the anti-Stokes field inside of the HFC:

$$E_{as} = \frac{-C_{as}^{4W} E_p E_p E_s^*}{L_{as}}. \quad (7)$$

To find the fields outside one end of the Raman cavity we multiply by $\frac{1}{2} \sqrt{T_{as}}$ where T_{as}

is the power transmission of the mirrors at the anti-Stokes wavelength since light can escape from either of two identical mirrors. The anti-Stokes field exiting the HFC

therefore takes the following form:

$$E_{as_f(b)} = -\frac{1}{2} \sqrt{T_{as}} \frac{C_{as}^{4W} E_p E_p E_s^*}{L_{as}} \quad (8)$$

Although it appears the process is more efficient for higher anti-Stokes mirror reflectivities (lower mirror losses, L_{as}), the field exiting the cavity is also scaled down by the transmission of the mirrors at the anti-Stokes frequency, thereby partially nullifying this effect. This is expected since the anti-Stokes generation is not a stimulated process.

The anti-Stokes field can be converted into power using the following equation[4,15,16]:

$$\Pi = \frac{1}{2} \sqrt{\frac{\epsilon_0}{\mu_0}} |E|^2 A \quad (9)$$

with the scaled area, A , for both the pump and the Stokes fields given by:

$$A = \frac{\ell \lambda_p}{4 \tan^{-1}\left(\frac{\ell}{b}\right)} \quad (10)$$

where ℓ is the length of the cavity and b is the confocal parameter of the beam. Using equations 7-10 we can calculate the ratio of the anti-Stokes power to Stokes power for the four-wave mixing process:

$$\%_{as} = \frac{T_{as}}{T_s} \left(\frac{C_{as}^{4W}}{L_{as}} \right)^2 |E_p|^4 \quad (11)$$

Equation 11 relates the coupling parameter, C_{as}^{4W} , to the anti-Stokes to Stokes power ratio, $\%_{as}$.

Figure-2 shows the predictions of equations 8-10 for constant pump frequency and a variable input pump power [17]. Note that the anti-Stokes power grows linearly with the Stokes power. This is a result of the self-limiting of the pump power inside the cavity above the Stokes laser threshold [4]. The measured ratio of the anti-Stokes to the Stokes power is 26 ppm on the Raman line center, which can be used to empirically determine the parameter C_{as}^{4W} in equation 7. The ratio of C_{as}^{4W} to G_s is 0.47. For perfect phase-matching this ratio becomes 1, thus for our configuration (equation 11), the anti-Stokes emission can be increased by a factor of 4. Figure-3 shows the predictions of equations 8-10 for a variable pump frequency and a constant input pump power of 3.3mW[17]. The anti-Stokes radiation is predicted to increase as the pump laser frequency is detuned to either side of the Raman resonance. This effect is due to the decreased Raman gain relative to the line-center value, which raises the cw Raman laser threshold. The resulting increased intra-cavity pump power initially increases the anti-

Stokes emission for detuning from line center. Eventually, the decreased Stokes emission dominates and the anti-Stokes generation falls as seen in figure-3.

Interferometric effects of the cavity at the anti-Stokes frequency can be accounted for by including the following cavity factor:

$$C(F, \delta) = \frac{1}{1 + F \cdot \sin^2 \frac{\delta}{2}} \quad (12)$$

where $F = \frac{4R_{as}}{(1 - R_{as})^2}$ and $\delta = \frac{\pi c}{\ell}(\Delta + \phi)$. ϕ corresponds to the relative frequency

difference between the Raman line-center and the anti-Stokes cavity resonance and Δ is the tuning of the pump frequency from the Raman line-center[18].

3. Experimental Apparatus

Figure-4 shows the experimental apparatus used to produce anti-Stokes emission. The cw Raman laser was optically pumped by a frequency-doubled Nd:YAG laser with single mode operation at 532nm with up to 200mW of optical power. Two Faraday isolators were used to minimize optical feedback to the pump laser. The beam was sent through a resonant phase modulator to place sidebands on the carrier frequency that were used for phase/frequency locking of the HFC and the pump laser. The phase and frequency of the laser were externally controlled by an electro-optic modulator (EOM) and acousto-optic modulator (AOM) [19]. The optical beam was passed through a lens pair for mode-matching the beam into the HFC. A half-wave plate and a polarizing beamsplitter (PBS) provided a variable attenuator for the pump power. A subsequent quarter-wave plate allowed the reflected beam from the HFC to be monitored for an error signal. A fast photodetector was used to measure the beat signal produced by the

reflected carrier frequency, sidebands and the leaked field from the HFC. The beat signal was given 30dB of gain before it was mixed to dc to produce the error signal. The error signal entered the servo, which sent slow corrections (DC-1kHz) to a piezo electric transducer (PZT) used to control the spacing of the HFC mirrors. Intermediate frequencies were sent to the AOM (10Hz-180kHz), while fast corrections were sent to the EOM (DC-800kHz). A small portion of the beam was diverted by a glass slide to monitor the pump power. In addition, the pump laser's frequency was monitored by a Burleigh wavemeter. A prism was used to spatially separate the pump (532nm), Stokes (683nm) and anti-Stokes (436nm) beams at the exit of the cavity. Photodetectors were used to monitor the powers of the output beams.

Figure-5 shows the measured anti-Stokes emission as a function of Stokes power produced for a constant pump frequency when the HFC is tuned to the Raman line center. As predicted by equations 6-8, the measured anti-Stokes power is observed to depend linearly on the generated Stokes power. A linear fit of the data was performed and the ratio of the anti-Stokes power to the Stokes power was measured to be 26 ppm. From this ratio, the anti-Stokes coupling coefficient, C_{as}^{4W} , was determined and used to fit the remaining data for this paper. Figure 6 shows the anti-Stokes emission as a function of pump power on line center. Fitting this dependence allows determination of the following experimental parameters: mirror reflectivities (transmissions) of 0.99979 (156ppm), 0.99977 (162ppm), and 0.24 (0.76) for the pump, Stokes, and anti-Stokes wavelengths respectively[20]. The measured Raman linewidth was 610MHz (FWHM), which corresponds to ~12 atm. of H₂[21]. The cavity length was 7.7 cm, the radius of curvature of the mirrors was 25cm, and the plane-wave gain coefficient was

$\alpha = 2.95 \times 10^{-9} \text{ cm/W}$ [22]. The Raman laser had a threshold of $830 \mu\text{W}$. Deviations from the theoretical fits at larger pump powers may result from the thermal heating of the gas due to the Raman process[6]. The parameters used in the fits for figures 5 and 6 are used for the remainder of this paper.

Figure-7 shows the measured anti-Stokes emission as a function of detuning from the Raman resonance. Also shown in the figure, as dashed and solid lines respectively, are the theoretical predictions for detuning with and without adjustment for the anti-Stokes cavity interference effects. Parameters for the overlaid theoretical plots were obtained using the fits of figures-5 and 6 with a pump power of 2.92 mW . The predictions of the theory including the anti-Stokes interference effects are in good agreement with the experimental data presented. For this theory, the anti-Stokes cavity resonance frequency was shifted by 100 MHz relative to the Raman line center, which gives the asymmetry in theoretical fit. The power reflectivity of the mirrors at the anti-Stokes wavelength was 24% .

The detuning of the pump laser from the Raman resonance was limited to $\pm 500 \text{ MHz}$ for two reasons. First, due to the double resonance requirement, the pump and the Stokes frequencies tune in the same direction, but at different rates.[23] For example, to tune across the Raman linewidth by an amount of 1 GHz , the pump laser needs to be tuned 4.5 GHz . Second, for a large detuning from the Raman linewidth the Raman laser can experience a mode-hop between adjacent transverse modes of the HFC.[23]

The spatial profile of the anti-Stokes emission on the Raman line center is shown in figure-8. The output was Gaussian, not a ring as typically seen. A narrow-band optical

filter caused the fringes in the spatial profile. The HFC behaves like a spatial filter and only allows one spatial mode of the pump and the Stokes beams to resonate. The experimental apparatus in this paper was configured such that the HFC was doubly resonant at the pump and Stokes wavelengths with fundamental Gaussian spatial profiles. The configuration therefore does not allow highly divergent Stokes rays to resonate. Higher order Stokes spatial modes may produce more efficient coupling of the pump and Stokes beams to the anti-Stokes beam, but this phenomenon was not investigated in the paper. Co-linear emission of anti-Stokes has been observed where self-induced phase matching in solid H₂ occurred [11]. In this system the Stokes frequency was detuned far-off the vibrational resonance which is not possible with the experimental apparatus of this paper.

4. Conclusions

Coherent cw anti-Stokes emission was observed. The four-wave mixing process producing the anti-Stokes radiation was modeled and the steady-state limit of the equations was investigated. For a constant pump frequency the cw anti-Stokes emission grew linearly with the Stokes output as predicted. The effects of tuning the pump frequency were also studied and the results are in good agreement with the presented theory when interferometric effects are included for the generated anti-Stokes. The cw anti-Stokes was co-linear to with the pump and the Stokes beam with a fundamental Gaussian spatial output. While an external power ratio of 26.3ppm was observed, higher ratios may be possible with a higher order, more divergent, Stokes spatial mode, or with different phase-matching mechanisms.

Acknowledgments:

This work is supported by a National Science Foundation grant PHY-9731602. We are grateful for the thoughts of Kai Drühl on stimulated anti-Stokes emission. We further thank Jan Hall and his group at JILA and Michael Jefferson at IBM for their help with electronics and phase/frequency locking.

References:

- [1] J. K. Brasseur, K. S. Repasky, and J. L. Carlsten, *Opt. Lett.* **23**, 367 (1998).
- [2] K. S. Repasky, J. K. Brasseur, L. Meng, and J. L. Carlsten, *J. Opt. Soc. Am. B*, **15**, 1667 (1998).
- [3] K. S. Repasky, L. Meng, J. K. Brasseur, J. L. Carlsten, and R. C. Swanson, *J. Opt. Soc. Am. B*, **16**, 717, (1999).
- [4] J. K. Brasseur, P. A. Roos, K. S. Repasky, and J. L. Carlsten, *J. Opt. Soc. Am. B*, **16**, 1305 (1999).
- [5] P. A. Roos, J. K. Brasseur, and J. L. Carlsten, *Opt. Lett.* **24**, 1130 (1999).
- [6] P. A. Roos, J. K. Brasseur, and J. L. Carlsten, “Intensity dependent refractive index in a non-resonant cw Raman laser due to thermal heating of the Raman-active gas” submitted to *JOSA B*.
- [7] J. L. Carlsten and T.J. McIlrath, *J. Phys. B*, **6**, L80 (1973).
- [8] W. R. Lempert, B. Zhang, R. B. Miles, and J. P. Looney, *J. Opt. Soc. Am. B*, **7**, 715 (1990).
- [9] H. Moriwaki, S. Wada, H. Tashiro, K. Toyoda, A. Kasai, and A. Nakamura, *J. Appl. Phys.* **74**, 2175 (1993).
- [10] A. Goehlich, U. Czarnetzki, and H. F. Döbele, *Applied Optics*, **37** 8453 (1998).

- [11] K. Hakuta, M. Suzuki, M. Katsuragawa, and J. Z. Li, Phys. Rev. Lett., **79**, 209 (1997).
- [12] Amnon Yariv, “Quantum Electronics,” 3rd edition, John Wiley and Sons, New York, (1989) p 474.
- [13] M. Scalora, S. Singh, and C. M. Bowden, Phys. Rev. Lett. **70**, 1248 (1993).
- [14] R. G. Harrison, Weiping Lu, and P. K. Gupta, Phys. Rev. Lett. **63**, 1372 (1989).
- [15] G. D. Boyd, W. D. Johnston, and I. P. Kaminow, J. of Quantum Electron., **QE-4**, 203 (1969).
- [16] In order to conserve energy the areas for the pump, Stokes and anti-Stokes beams, used to calculate power, need to be identical and are normalized to the pump beam. The wavelength dependence of the area for the Stokes beam is included in the mode filling parameter of reference 15.
- [17] All of the fits used the following parameters: $\lambda_{p(s)}= 532\text{nm}$ (683nm), $\lambda_{as}=435\text{nm}$, $\alpha = 2.95 \times 10^{-9} \text{ cm/W}$, $R_{p(f)} = R_{p(b)} = 0.99979$, $R_{s(f)} = R_{s(b)} = 0.99977$, $R_{as} = 0.24$, $T_{p(f)} = 156 \text{ ppm}$, $T_s = 163 \text{ ppm}$, $T_{as} = 0.76$, $\ell = 7.68 \text{ cm}$, $b=18\text{cm}$, Raman linewidth, Γ , is 610MHz (FWHM) and the anti-Stokes to Stokes power ratio is 26ppm.
- [18] Max Born and Emil Wolf, “Principles of Optics,” 6th edition, Cambridge University Press, New York, (1980) page 327.
- [19] J. L. Hall, and T. W. Hänsch, Opt. Lett., **9**, 502 (1984).
- [20] The values for the pump and Stokes mirror reflectivities were measured by a cavity ring-down. The values are $R_{p(s)}=0.99979 \pm 0.00001$ (0.99977 ± 0.00001). The transmissions were $T_p=(153 \pm 8)\text{ppm}$, and $T_s=(150 \pm 20)\text{ppm}$.

- [21] W. K. Bischel and M. J. Dyer, Phys. Rev. A., **33**, 3113 (1986).
- [22] W. K. Bischel and M. J. Dyer, J. Opt. Soc. Am. B **3**, 677 (1986).
- [23] J.K. Brasseur, P.A. Roos, and J.L. Carlsten, "Frequency tuning characteristics of a continuous wave Raman laser in H₂." Submitted to JOSA B.

Figure Captions

1. The energy level diagram for the cw coherent anti-Stokes process.
2. The predictions of equations 7-9 for anti-Stokes emission with a constant pump frequency with a variable pump power. The Stokes output is overlaid to illustrate the linear relationship between Stokes and anti-Stokes outputs.
3. The predictions of equations 4 and 7-9 for anti-Stokes emission as a function of detuning from the Raman linewidth at a pump power of 3.32mW. The predicted Stokes emission is overlaid for reference.
4. The apparatus used to create cw coherent anti-Stokes emission.
5. The output power of the cw anti-Stokes emission vs. the output Stokes power. The linear fit gives the anti-Stokes to Stokes power ratio of 26ppm.
6. The anti-Stokes emission as a function of pump power with the predictions of equations 7-9 overlaid.
7. The anti-Stokes emission as a function of detuning from the Raman resonance with a pump power of 2.92mW with the predictions of equations 4 and 7-9 overlaid with (solid) and without (dashed) the interferometric effects.
8. The spatial profile of the cw anti-Stokes beam at the exit of HFC after a narrow-band filter.

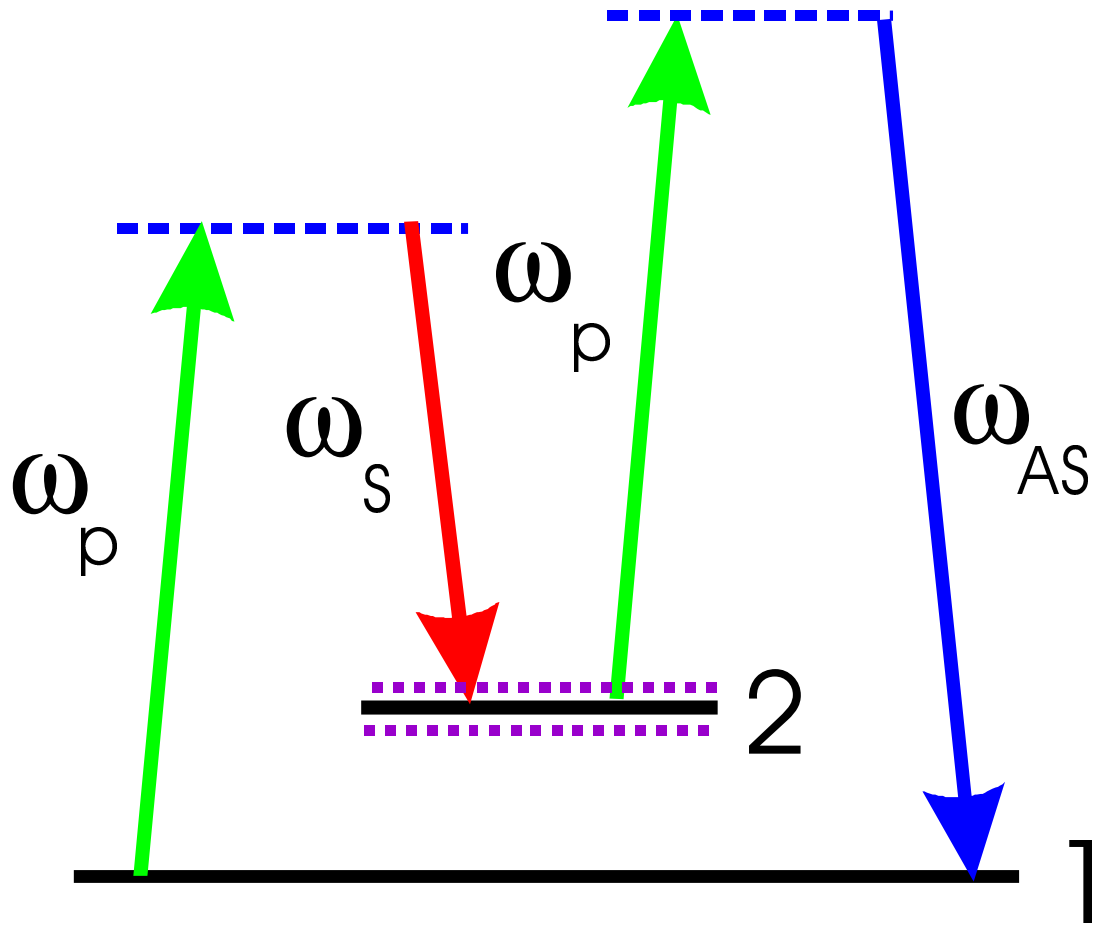


Figure-1

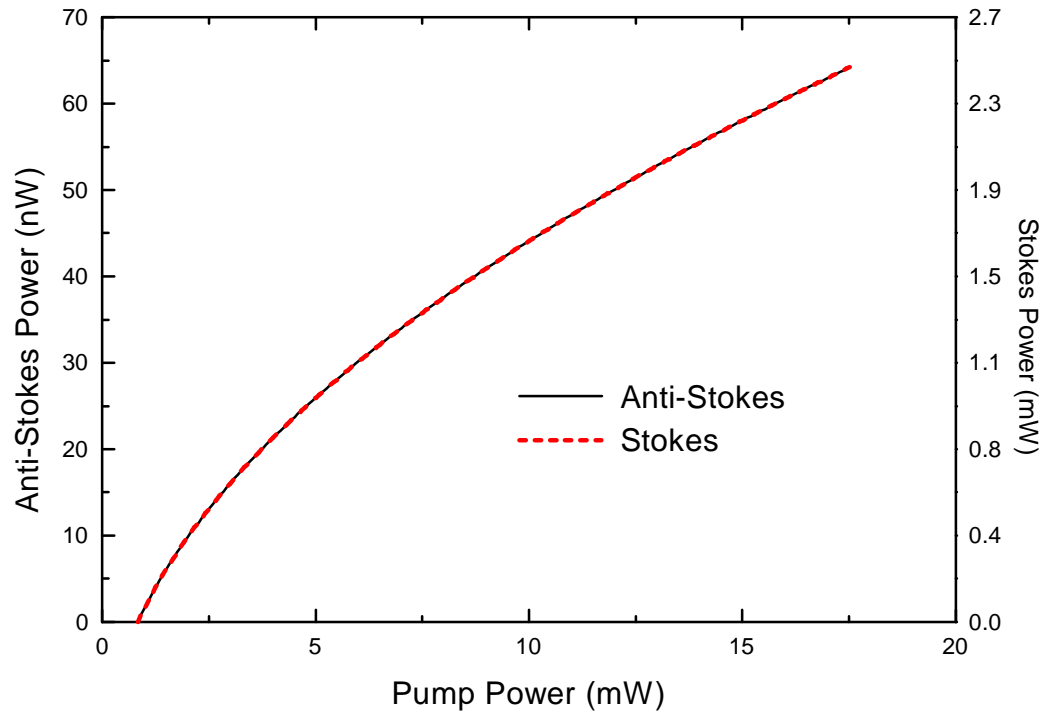


Figure-2

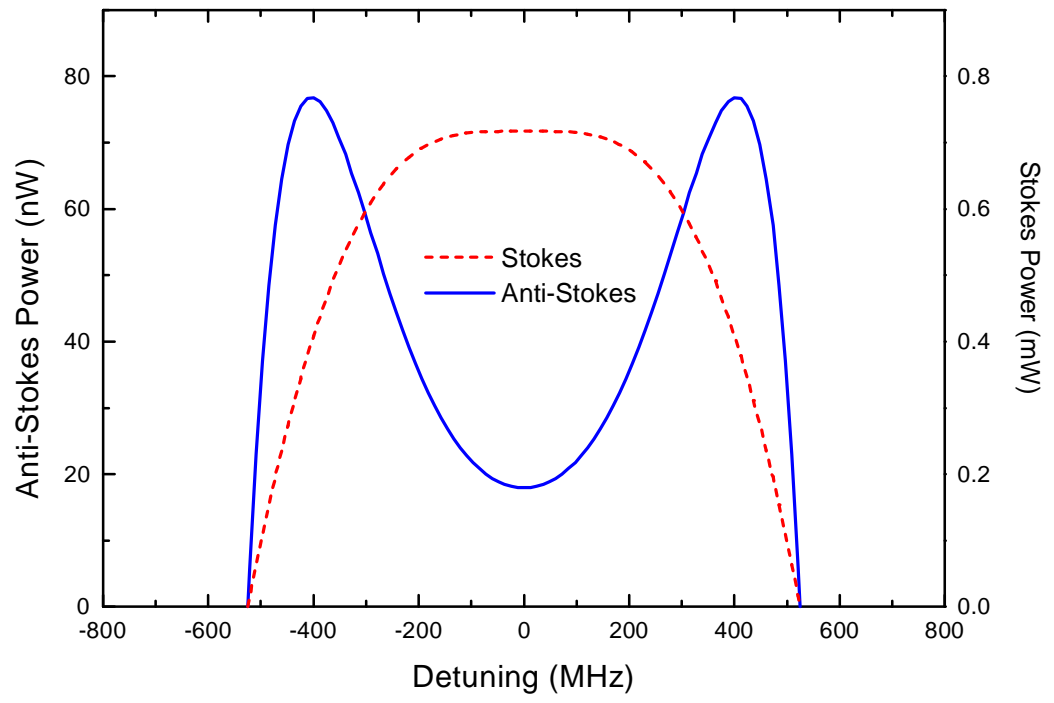


Figure-3

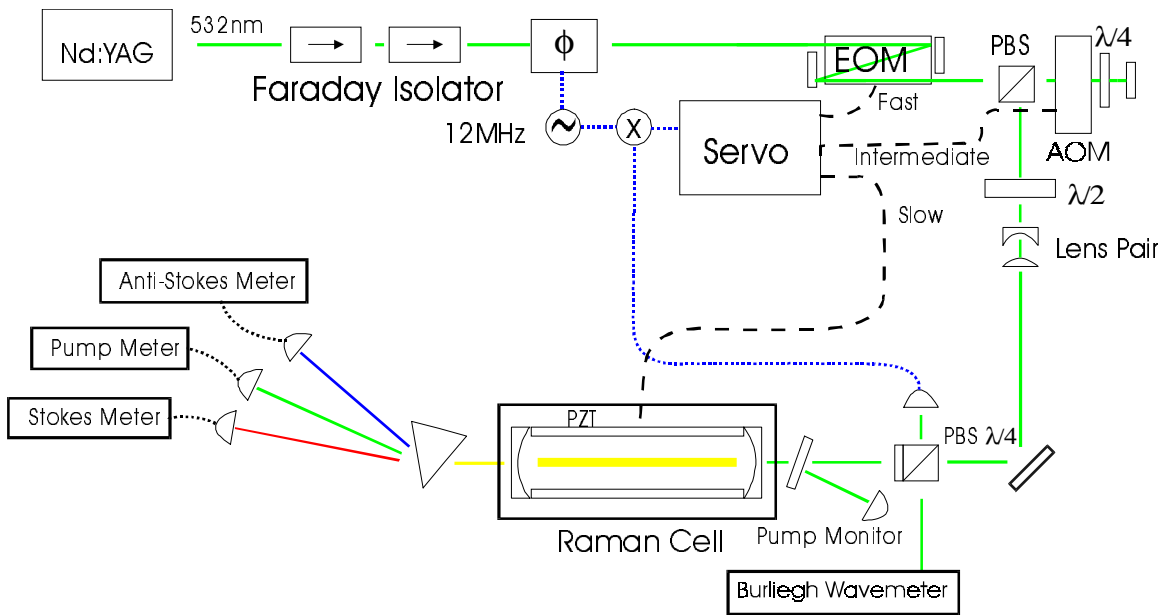


Figure-4

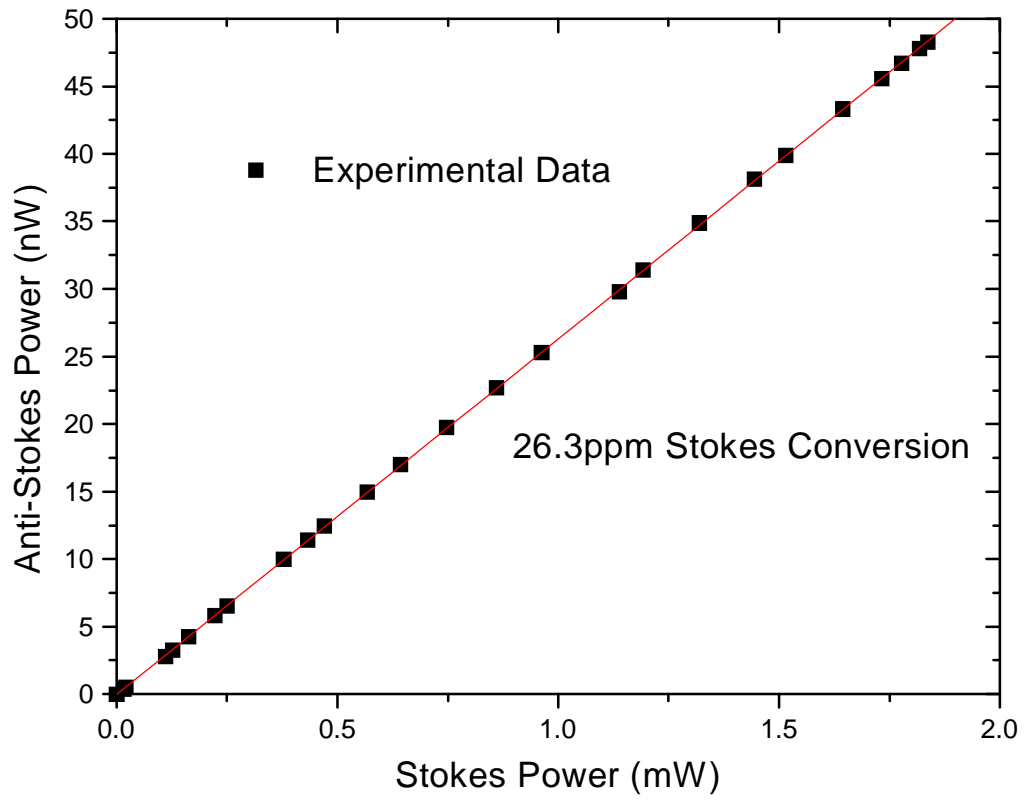


Figure-5

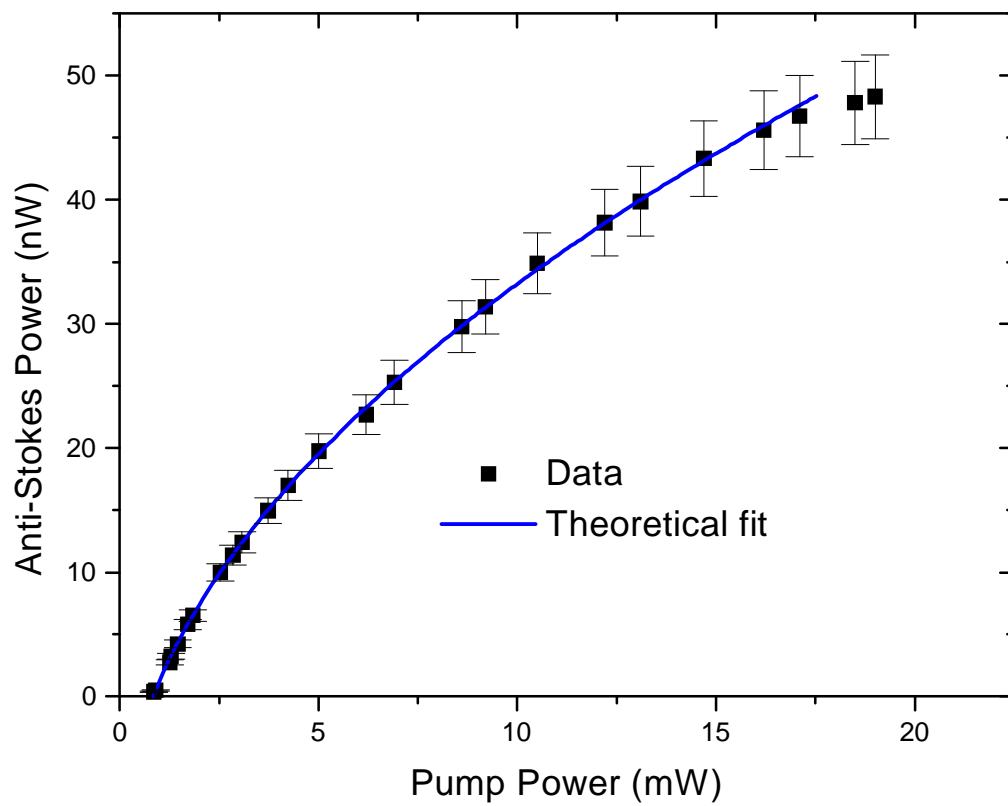


Figure-6

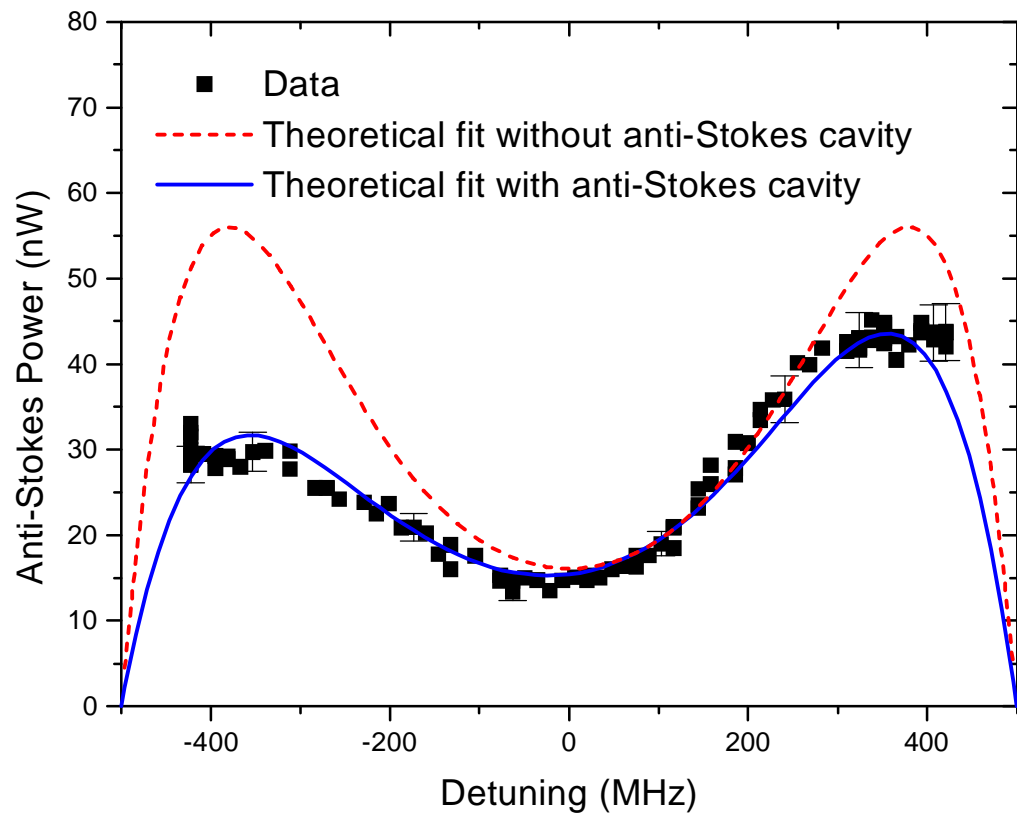


Figure-7

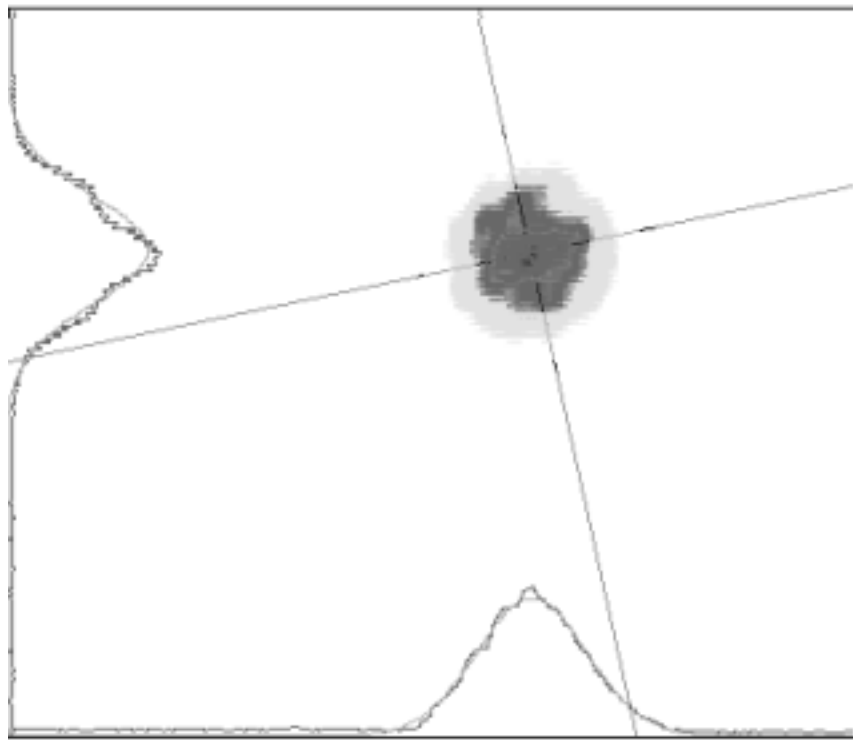


Figure-8